Available online at www.sciencedirect.com
SCIENCE DIRECT®
International Journal of Thermal Sciences 43 (2004) 791–796
International Journal of Thermal Sciences
www.elsevier.com/locate/ijts

Poiseuille–Benard instability in a horizontal rectangular duct water flow

Christophe Bonnefoi, Chérifa Abid *, Marc Medale, François Papini

Ecole polytechnique universitaire de Marseille, IUSTI U.M.R CNRS N° 6595, technopole de Château-Gombert, 5, rue Enrico Fermi, 13453 Marseille cedex 13, France

Received 20 August 2003; received in revised form 15 February 2004; accepted 24 February 2004

Available online 10 June 2004

Abstract

The aim of the present study is to investigate thermoconvective instabilities in a mixed convection phenomenon. The flow of an incompressible fluid (water) in a horizontal rectangular duct, uniformly heated from below (Poiseuille–Benard flow) was considered. Many experiments were conducted for a wide range of fluid velocities (Reynolds number) and heat fluxes supplied to the wall (Richardson number) in order to describe and to analyse these instabilities. Experimental results enabled us to distinguish several regimes of flow and particularly the domains of thermoconvective instability. Using fluid temperature measurement, a stability diagram was established in a [Re, $Re\,Ri$] plane; this diagram shows the various regimes. In parallel, a direct numerical simulation, which solves the Navier–Stokes equations coupled with energy equation, was carried out. The computations helped us to identify and thus better understand the possible basic mechanisms leading to the quite complex fluid flow observed, which results in the combination of the forced fluid flow and the buoyancy-induced flow. In the range of parameters under consideration, the fluid flow structure is mainly composed of two longitudinal rolls, which interact dynamically once a threshold has been reached.

Keywords: Mixed convection; Water flow; Thermoconvective instabilities; Horizontal duct

1. Introduction

This paper deals with thermal instabilities occurring in a mixed convection phenomenon. It concerns an incompressible flow in a horizontal rectangular duct heated from below. Heat flux supplied to the fluid induces a secondary flow, which is superimposed on the main forced flow.

Mixed convection flow in horizontal ducts has been widely studied [1–6]. During the first half of the twentieth century, research on this subject attempted to explain certain meteorological phenomena. More recently applications have been concerned with technological processes such as the cooling of electronic components or the production of thin films in CVD reactors; these works have mainly focused on the heat transfer enhancement related to thermoconvective structures in the flow. Results of the linear hydrodynamic stability theory have shown that the thermally stratified Poiseuille flow remains stable as long as the Rayleigh number Ra does not exceed a certain critical value, i.e., $Ra^* = 1708$. Beyond this value, the basic flow becomes unstable and two kinds of thermoconvective structures, called "transversal rolls" and "longitudinal rolls", may appear. Such results concern the case of constant temperatures imposed at the upper and lower horizontal faces of the channel; of course the upper part is colder than the lower one. The aim of our study is to investigate thermoconvective instabilities in the case of an imposed heat flux at the lower horizontal wall. This work was undertaken with a combined approach linking experiments and numerical simulations.

2. Experimental set-up

Our experimental device (see Fig. 1) was a horizontal rectangular duct uniformly heated from below. This channel was 14 mm high, 26 mm wide and 2 m long; its 3 mm thick walls were made of Plexiglas. The first part of the

* Corresponding author.
E-mail addresses: christophe.bonnefoi@polytech.univ-mrs.fr (C. Bonnefoi), cherifa.abid@polytech.univ-mrs.fr (C. Abid), marc.medale@polytech.univ-mrs.fr (M. Medale), francois.papini@polytech.univ-mrs.fr (F. Papini).

1290-0729/$ – see front matter
doi:10.1016/j.ijthermalsci.2004.02.019

Nomenclature

D_h	$= 4S/P$ hydraulic diameter of the channel (S: cross-section area, P: cross-section perimeter)	$\vec{V}$	non-dimensional velocity vector (v_{ref}: reference velocity associated to natural convection alone)
g	gravity acceleration	t	time
Gr	$= g\beta\Delta T h^3/\mu\kappa$] Grashoff number	β	Volumetric expansion coefficient
h	height of the channel (14 mm)	φ	Applied heat flux at the lower horizontal surface
l	length of the channel (560 mm)	T_i	Temperature at the inlet of the test section
$\vec{n}$	outward unit vector normal to the domain boundary	T_o	Average temperature at the outlet of the test section
p	dynamical pressure ($P_{\text{hydrostatic}}$: hydrostatic pressure at the outlet)	$\Delta T'$	temperature difference between the heated wall and the inlet fluid (T_i)
Pr	$= \nu/\kappa$ Prandtl number	κ	thermal diffusivity of the liquid
Re	$= V D_h/\nu$ Reynolds number (V: average inlet velocity)	μ	dynamic viscosity of the liquid
Ri	$= g\beta\Delta T L/V^2$ Richardson number	ν	kinematic viscosity of the liquid
		θ	$= \frac{T-T_i}{\Delta T}$ non-dimensional temperature
		$\bar{\bar{\sigma}}$	stress tensor for the Newtonian liquid

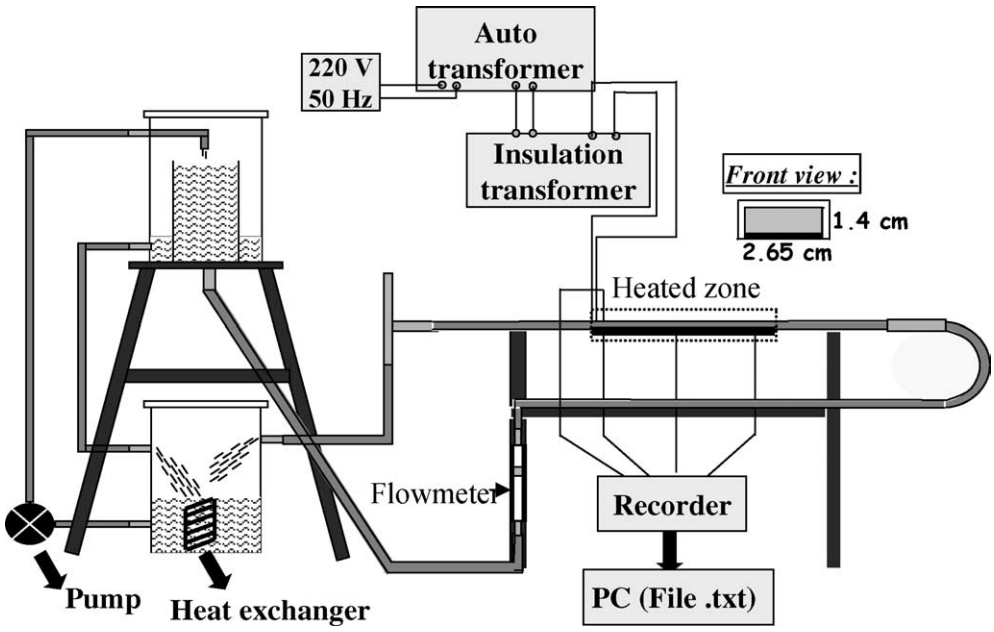

Fig. 1. Experimental set-up.

channel was designed to enable the isothermal inlet fluid flow to be fully developed so that a Poiseuille type flow was obtained at the inlet of the test zone. Next to this section was the central testing zone, which was heated from below over a length of 0.56 m through the lower wall made of copper with electrical resistance is 93.1 Ohms. Heating is produced by Joules effect whereby a direct electric current is applied between the input and output terminals. The strength could vary from 0.1 to 2 A. Thus the heat flux φ was uniform throughout the straight section of the testing zone and could vary from 76 $\text{W}\cdot\text{m}^{-2}$ to 30 $\text{kW}\cdot\text{m}^{-2}$. The inlet fluid temperature was maintained constant and equal to 20 °C by means of an external heat exchanger. A multistage centrifugal pump (flow rate 25 $\text{l}\cdot\text{mn}^{-1}$) ensured fluid circulation. The average fluid velocity v was regulated by a flow meter.

Finally the experimental device enabled us to measure local fluid temperature (by means of K-type thermocouples) in several longitudinal locations ($x = 200, 400, 500$ mm) and at various heights in the duct (0–14 mm). For this purpose thermocouples were inserted inside syringes in order to enable us to slide them into the section. Several series of measurements were carried out in order to cover a wide range of fluid flow rates (Reynolds number ranging from 100 to 2000) and applied heat fluxes (φ ranging from 0.1 to 15 $\text{kW}\cdot\text{m}^{-2}$).

3. Experimental results

We remind the reader that Reynolds and Richardson numbers are calculated using the physical properties of water determined at the average temperature $((T_o + T_i)/2)$ between the inlet and the outlet of the testing zone (Reynolds number $Re = \frac{V D_h}{\nu}$ where V is fluid velocity, D_h hydraulical diameter and ν kinematic viscosity; and Richarson number $Ri = \frac{g\beta\Delta T L}{V^2}$ where g is gravitational acceleration, β the thermal expansion coefficient, $\Delta T = T_o - T_i$ the difference in fluid temperature difference between the inlet and outlet of the heated zone and L the length of the heated zone).

Fig. 2 shows the evolution of the fluid temperature versus the vertical distance from the upper horizontal wall ($Z = 0$ for the top of the cross section and $Z = 14$ mm for the bottom). Experimental conditions were as follows: longitudinal coordinate $x = 400$ mm, fluid velocity $V = 10.9$ mm·s^{-1} ($Re = 200$) and heat flux $\varphi = 1.9$ kW·m^{-2}. The temperature variation, according to the vertical coordinate, shows that on average the fluid temperature is higher at the top than in the centre of the cross-section. This shows that the mixed convection phenomenon is installed. In fact the fluid heated in the lower part of the section, being lighter, rises towards the upper part of the cross-section. The colder and therefore heavier fluid at the top moves down by gravitation towards the lower part. Thus we have the formation of convective rolls.

For the same fluid velocity (Reynolds number) and for different values of heat flux supplied to the wall, Figs. 3(a) and (b) show fluid temperature signals for two different Z values (respectively for the top $Z = 2$ mm and the bottom $Z = 13$ mm). In this case, experimental conditions are as follows: longitudinal coordinate $x = 400$ mm, fluid velocity $V = 1.09$ cm·s^{-1} ($Re = 200$) and heat flux values are: 0.47, 1.9 and 7.6 kW·m^{-2}. From these figures we can say that, for a constant Re number, when we increase the heat flux an instability phenomenon appears. The latter manifests itself through the appearance of temporal fluctuations of large amplitude in the fluid temperature. For $\varphi = 0.47$ kW·m^{-2} the signal is stable and for higher values of φ, the instability appears with an increasing of its amplitude as φ rises. Elsewhere the instability phenomenon seems to begin in the boundary layer in the lower part of the cross section. The numerical study, conducted in parallel highlights this instability mechanism.

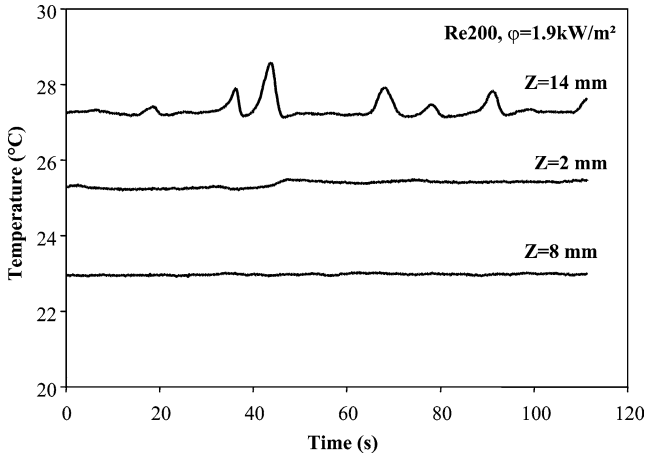

Fig. 2. Fluid temperature evolution versus Z.

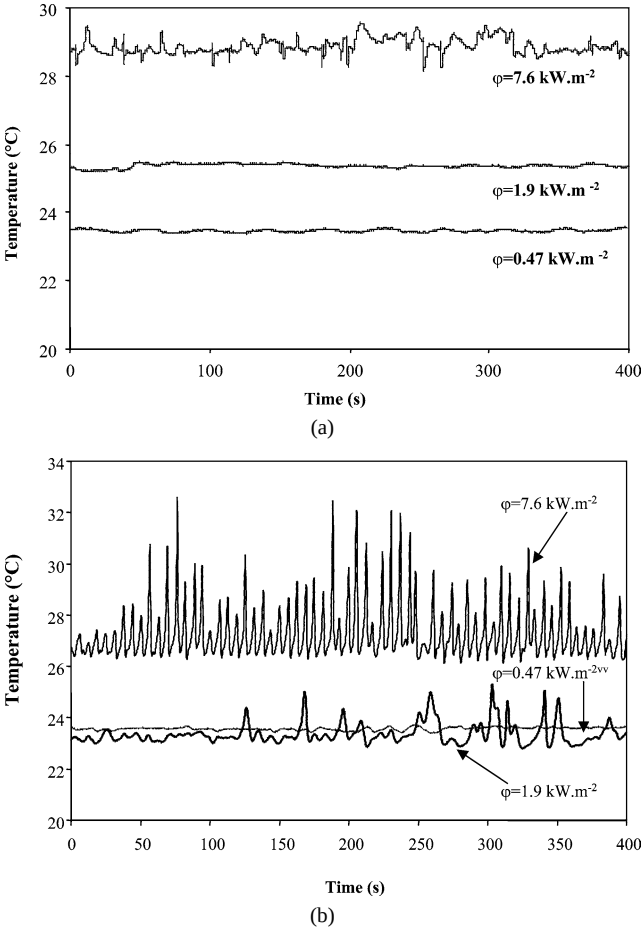

Fig. 3. (a) Fluid temperature evolution for various heat fluxes supplied to the wall (top $Z = 2$ mm); (b) Fluid temperature evolution for various heat fluxes supplied to the wall (bottom $Z = 13$ mm).

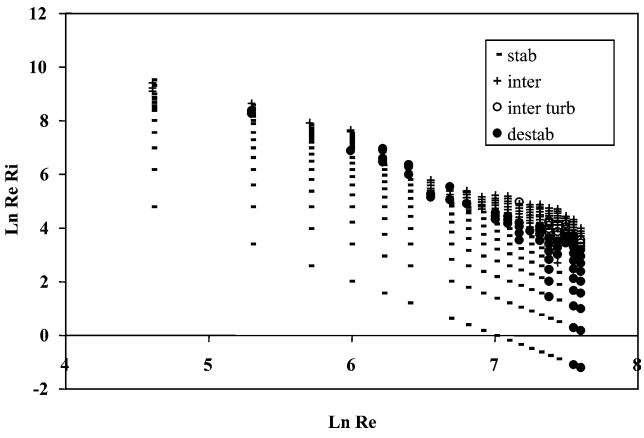

Fig. 4. Stability diagram.

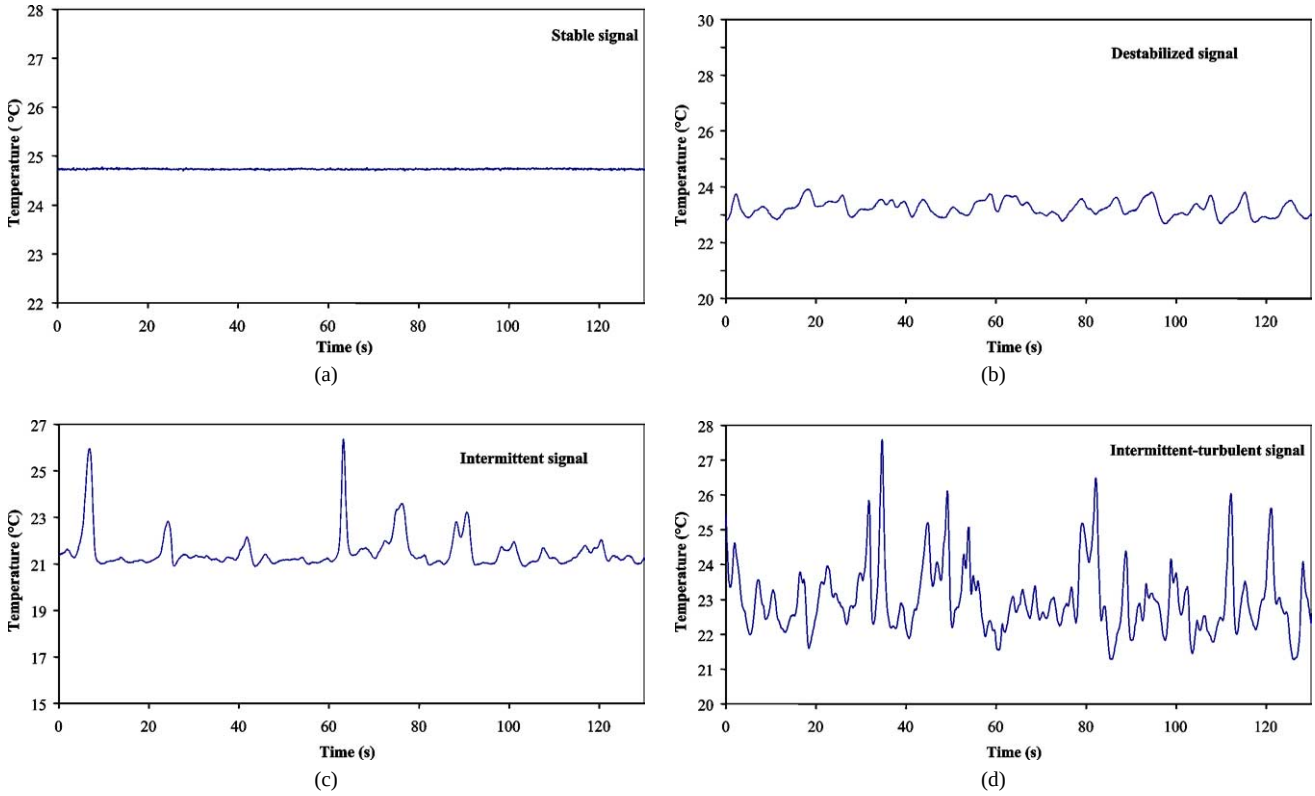

Fig. 5. (a) Stable signal; (b) Destabilized signal; (c) Intermittent signal; (d) Intermittent-turbulent signal.

The results obtained in the range of parameters considered in this study, allow us to highlight various regimes and in particular a domain of thermoconvective instabilities. Thus a stability diagram was established (see Fig. 4) and typical signals are presented in Figs. 5(a)–(d).

4. Numerical approach

In parallel to these experiments, direct numerical simulations were conducted on the basis of the coupled set of Navier–Stokes and energy equations.

4.1. Governing equations

The problem under consideration is governed by the coupled incompressible Navier–Stokes and energy equations [7]. Nevertheless, since we assume the Boussinesq approximation stands, this implies considering numerically only moderate heating configurations. Introducing the dimensionless variables of space, velocity, time and temperature, built respectively on the height of the channel (h), the natural convection velocity ($v_{\text{ref}} = (g\beta\Delta T h)^{1/2}$), the natural convection time scale (h/v_{ref}) and the temperature difference ($\Delta T'$), the conservation equations read as follows:

Energy conservation equation in the water flow:

$$\sqrt{Gr}\cdot Pr\cdot\left[\frac{\partial\theta}{\partial t}+\left(\vec{v}\cdot\vec{\nabla}\right)\theta\right]=\vec{\nabla}^2\theta \tag{1}$$

Associated with the thermal boundary conditions:

- At the inlet: $\theta = 0$;
- At the lower horizontal wall: either $\theta = 1$ or $\frac{\partial\theta}{\partial n} = \bar{\varphi}_{\text{adim}}$;
- At the three other lateral walls: $\frac{\partial\theta}{\partial n} = 0$.

Initial condition: uniform temperature field $\theta(x, y, z, 0) = 0$.

For the incompressible fluid flow in the liquid domain:

$$\vec{\nabla}\cdot\vec{v}=0;$$

$$\sqrt{Gr}\cdot\left[\frac{\partial\vec{v}}{\partial t}+\left(\vec{v}\cdot\vec{\nabla}\right)\vec{v}\right]=-\vec{\nabla}p+\vec{\nabla}^2\vec{v}+\sqrt{Gr}\,\theta\vec{z}$$

Associated with the fluid flow boundary conditions:

- At the inlet: $\vec{v}(x=0, y, z) = Re\cdot\vec{v}^{\text{adim}}_{\text{Poiseuille}}$;
- At the lateral walls: $\vec{v} = \vec{0}$;
- At the outlet: $\vec{n}\cdot\bar{\bar{\sigma}}\cdot\vec{n} = p_{\text{hydrostatic}}$.

Initial condition: uniform velocity field $\vec{v}(x, y, z, 0) = \vec{0}$.

4.2. Numerical model

The 3D numerical model we developed to solve the coupled fluid flow and heat transfer problem is based on the finite element method [7]. First of all, a segregated approach is used to build up separate integral forms associated on the one hand with the incompressible fluid flow

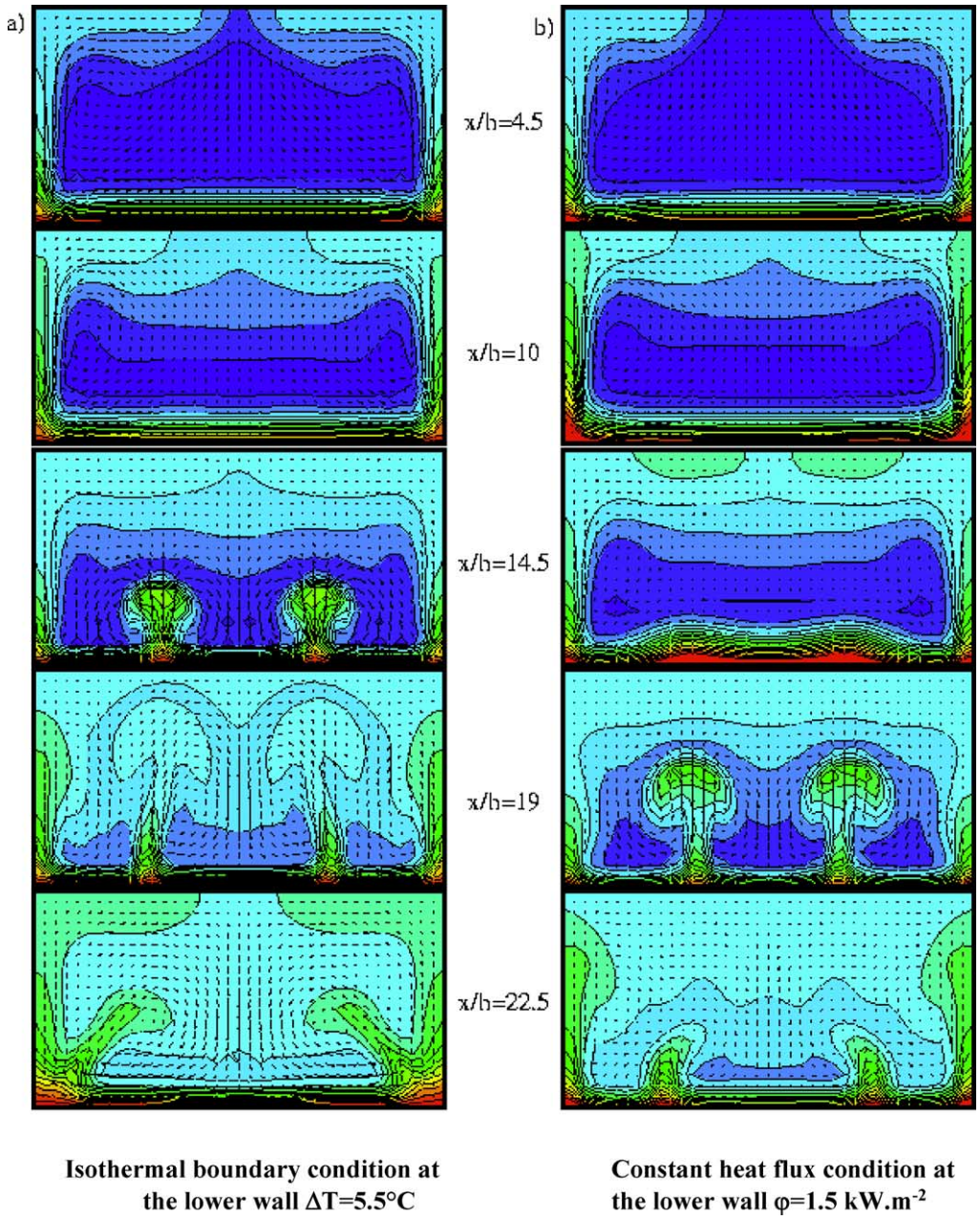

Fig. 6. Flow structure.

problem, and the heat transfer problem on the other hand. The former is written in a primary variable formulation and is solved using an unconditionally stable projection algorithm [8]. Then the spatial discretisation is achieved using tri-quadratic hexahedral finite elements for the velocity and temperature variables, whereas tri-linear approximation is used for pressure. Time integration is performed with the classical first order backward Euler scheme. At each time step the three algebraic systems related momentum, incompressible projection and energy conservation are solved with iterative solvers provided in the Pestc toolkit [9], running high performance massively parallel computers (IBM SP3 and SP4).

4.3. Numerical simulations

The two basic configurations we considered in our preliminary numerical simulations differ mainly in the way the heating system along the lower horizontal wall is taken into account: constant temperature or constant heat flux. We have carried out unsteady numerical computations in these two configurations, for $Re = 200$ and, on the one hand, $\Delta T'$ ranging from 1 to 6 °C or, on the other hand, φ ranging from 1 to 2 kW·m^{-2}.

In Fig. 6, one can observe that the main feature of the fluid flow structure is quite comparable, but already complex. Indeed, a secondary flow takes place in the first part of the

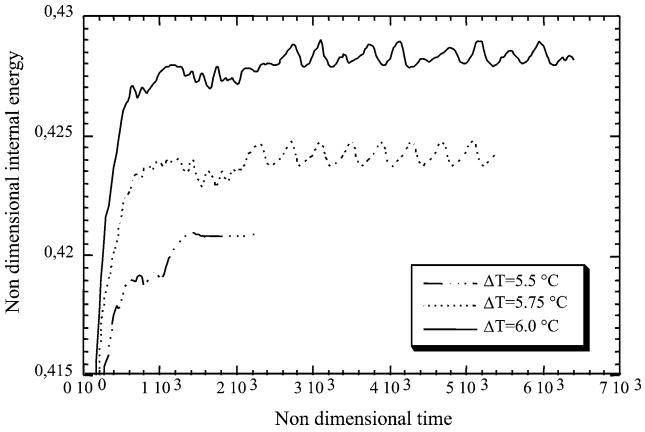

Fig. 7. Non-dimensional internal energy evolution for various isothermal conditions.

channel (inlet at $x/h = 0$, left of the picture), consisting of two longitudinal rolls rotating in opposite directions (upward at the lateral wall). Close to the half-length of the channel, a new disturbance gives rise to two hot spots (which have a mushroom shape in the cross section of the fluid flow) equally distributed in the transverse direction of the channel. The secondary flow in the cross section is significantly modified, but is strong enough to reach the last part of the channel where the mushroom-like hot spots are displaced toward the vertical lateral walls. These results also reveal that the configuration of constant heat flux reaches the unsteadiness limit at a lower level of energy transferred to the fluid than in the isothermal case.

In the isothermal heating model, we found a threshold ($5.5 < \Delta T' < 5.6$) which distinguishes the configurations in which a steady solution exists from those where only unsteady solutions were found (periodic just above the threshold, and dynamically more complex when further along). In the constant heat flux model, we also found a transition to the dynamical regime (close to $\varphi = 1.6\ \mathrm{kW{\cdot}m^{-2}}$), but unlike in the former case we did not found any periodic behaviour. This result is shown in Fig. 7 where the non-dimensional internal energy is presented for various isothermal conditions applied to the lower wall.

5. Conclusion

This work on a mixed convection phenomenon was undertaken with a combined approach linking experiments and numerical simulations. Experimental results enabled us to distinguish several regimes of flow and particularly the thermoconvective instability domains. The computations helped us to identify and thus better understand the possible basic mechanisms leading to the quite complex fluid flow observed, which results in the combination of the forced fluid flow and the buoyancy-induced flow. In the range of parameters under consideration, the fluid flow structure is mainly composed of two longitudinal rolls, which interact dynamically once a threshold has been reached. Moreover, we also show the influence of the two thermal boundary condition models (isothermal or constant flux) on the fluid flow and related heat transfer.

Acknowledgements

Authors would like to thank the CNRS for providing substantial computer resources on its high performance computers (IBM SP3 and SP4) at IDRIS, Orsay, France.

References

[1] R.E. Kelly, The onset and development of Rayleigh–Bénard convection in shear flow: A review, in: D.B. Spaulding (Ed.), Physicochemical Hydrodynamics, Advance Publication, London, 1977.
[2] C. Abid, F. Papini, Thermal instabilities in a mixed convection phenomenon: Nonlinear dynamics, Phys. Rev. E 56 (6) (1997) 6735–6744.
[3] X. Nicolas, Revue bibliographique sur les écoulements de Poiseuille–Rayleigh–Bénard : Écoulements de convection mixte en conduites rectangulaires horizontales chauffées par le bas, IJTS 41 (2002) 961–1016.
[4] C.H. Yu, M.Y. Chang, T.F. Lin, Structures of moving transverse and mixed rolls in mixed convection of air in a horizontal plane channel, Internat. J. Heat Mass Transfer 40 (1997) 333–346.
[5] J.M. Luijkx, J.K. Platten, J.C. Legros, On the existence of thermoconvective rolls transverse to a superimposed mean Poiseuille flow, Internat. J. Heat Mass Transfer 24 (1981) 803–817.
[6] M.T. Ouazzani, J.K. Platten, A. Mojtabi, Intermittent patterns in mixed convection, Appl. Sci. Res. 51 (1993) 677–685.
[7] M. Médale, Simulation numérique d'écoulements thermo-convectifs et à interfaces mobiles, H.D.R. Thesis, Marseille, 2000.
[8] J.L. Guermond, L. Quartapelle, Calculation of incompressible viscous flows by an unconditionally stable projection FEM, J. Comput. Phys. 132 (1997) 12–33.
[9] S. Balay, W. Gropp, L.C. McInnes, B. Smith, PETSc 2.0.21 Users Manual, Mathematics and Computer Science Division, Argone National Laboratory, 1998.